PHYSICAL REVIEW B **88**, 140406(R) (2013)

Giant enhancement of spin pumping efficiency using Fe_3Si ferromagnet

Y. Ando,[1,*] K. Ichiba,[1] S. Yamada,[2] E. Shikoh,[1] T. Shinjo,[1] K. Hamaya,[2] and M. Shiraishi[1]
[1]*Graduate School of Engineering Science, Osaka University, Osaka, Japan*
[2]*Department of Electronics, Kyushu University, Fukuoka, Japan*

(Received 21 May 2013; revised manuscript received 3 September 2013; published 28 October 2013)

The generation, propagation, and control of spin current have attracted a great deal of attention because of the possibility of realizing dissipation-free information propagation. Although electrical generation of spin current originally made significant advances in spin-current devices, novel spin-current-generation approaches without the application of charge current, such as dynamical methods, have also been gaining importance. However, the low spin-current generation efficiency associated with dynamical methods has impeded further progress towards practical spin devices. Here we show that by introducing a single-crystalline ferromagnetic material, Fe_3Si, pure spin currents can be generated about 20 times more efficiently when using a dynamical method. This achievement paves the way to the development of different spin-based devices.

DOI: 10.1103/PhysRevB.88.140406 PACS number(s): 72.25.Ba, 72.25.Mk

While steady progress has been made in the application of electrical methods for spin-current generation in spintronic devices,[1–4] recent studies have also focused on more radical approaches such as dynamical,[5–15] thermal,[16] and acoustic[17] methods. These methods are expected to pave the way for a new generation of novel spintronics devices that involve no charge current. Spin pumping is a dynamical method in which a spin current is generated by a precession of the magnetization.[5–15] It has been the subject of considerable interest because a spin current can be produced over a large area without the presence of a charge current, which is expected to reduce the problem of conductance mismatch.[10] Although spin pumping is a promising technique for next generation spin-current devices, the low efficiency of the generation of pure spin current impedes further progress towards practical spin devices.[4,9,18] [see Supplemental Material (SM) A (Ref. 19)] For this reason, identifying a novel ferromagnetic (FM) material that is capable of highly efficient spin injection is of the utmost importance. Here, we focus on single-crystal Fe_3Si, which has desirable properties such as a smaller Gilbert damping constant and a larger resistivity than those for $Ni_{80}Fe_{20}$ (Py), the most commonly used spin source.[8,9] Moreover, high-quality single-crystal Fe_3Si can be easily grown on semiconducting substrates such as Si, Ge, and GaAs with atomically flat interfaces.[20–24] This means that Fe_3Si can be applied to a wide variety of materials, allowing the development of novel semiconductor-based spintronic devices in addition to metal-based devices. In the present Rapid Communication, an enhancement of spin-injection efficiency, about 20 times of that for a conventional spin injector such as Py, is demonstrated by using a single-crystal Fe_3Si layer. It should be noted that the enhancement mechanism of this study is compatible with conventional ones such as the utilization of half-metal materials, optimization of the resistance, reduction of the Gilbert damping constant, etc.

A 25-nm-thick Fe_3Si epitaxial layer was grown on a high-resistivity float zone (FZ)-Si(111) substrate by molecular beam epitaxy (MBE) at room temperature.[20,21] After cleaning the substrate with an aqueous HF solution ($HF:H_2O = 1:40$), a heat treatment was carried out at 450 °C for 20 min. in a molecular beam epitaxy (MBE) reaction chamber with a base pressure of 2×10^{-9} Torr. Cross-sectional transmission electron microscopy observations reveal that the interface in the Fe_3Si samples is atomically flat [see Fig. 4(a) and Ref. 20]. A 5-nm-thick Pd layer was then formed by electron beam (EB) evaporation at room temperature. Two lead wires (separated by a $w = 1.0$ mm gap) for measuring the dc electromotive force were attached to the edge of the Pd film using Ag paste. During the measurements, microwaves with a frequency of 9.61 ± 0.01 GHz were generated in a TE_{102} cavity of an electron spin resonance (ESR) system (Bruker EMX10/12), and an external static magnetic field H was applied at an angle θ_H, as shown in Fig. 1(a). The sample was placed inside the cavity in a nodal position where the rf electric and magnetic field components were a minimum and a maximum, respectively. The dc electromotive force V_{EMF} was measured using a nanovoltmeter. All measurements were carried out at room temperature.

Figure 1(b) shows ferromagnetic resonance (FMR) spectra, i.e., $dI(H)/dH$ as a function of H-H_{FMR}, for the Pd/Fe_3Si/Si sample recorded at $\theta_H = 0°$, 80°, 110°, and 180°, where I, H, and H_{FMR} are the microwave absorption intensity, external magnetic field, and FMR field, respectively. However, FMR could not be measured at $\theta_H = 90°$ due to the limited external magnetic field strength, i.e., the maximum magnetic field of 1.3 T in the ESR system is smaller than the anisotropy field for the Fe_3Si thin film (~1.5 T). For $\theta_H = 0°$, 80°, 110°, and 180°, clear FMR spectra were observed. From the obtained resonant magnetic field ($H_{FMR} = 92.9$ mT) at $\theta_H = 0°$, the saturation magnetization M_s is estimated to be 828 emu/cc, which is consistent with previously measured values using a vibrating sample magnetometer,[20,25] indicating that the spectra are associated with FMR in the Fe_3Si layer. Figure 1(c) shows V_{EMF}/w as a function of H-H_{FMR}. For $\theta_H = 0°$, a clear signal can be seen at the FMR condition. The EMF signals were analyzed using a deconvoluted fitting function with independent contributions from the inverse spin Hall effect (ISHE, symmetrical Lorentzian curve centered on H_{FMR}) and the anomalous Hall effect (AHE, asymmetrical curve) as follows:[8]

$$V_{EMF} = V_{ISHE}\frac{\Gamma^2}{(H - H_{FMR})^2 + \Gamma^2} + V_{AHE}\frac{-2\Gamma(H - H_{FMR})}{(H - H_{FMR})^2 + \Gamma^2}, \quad (1)$$

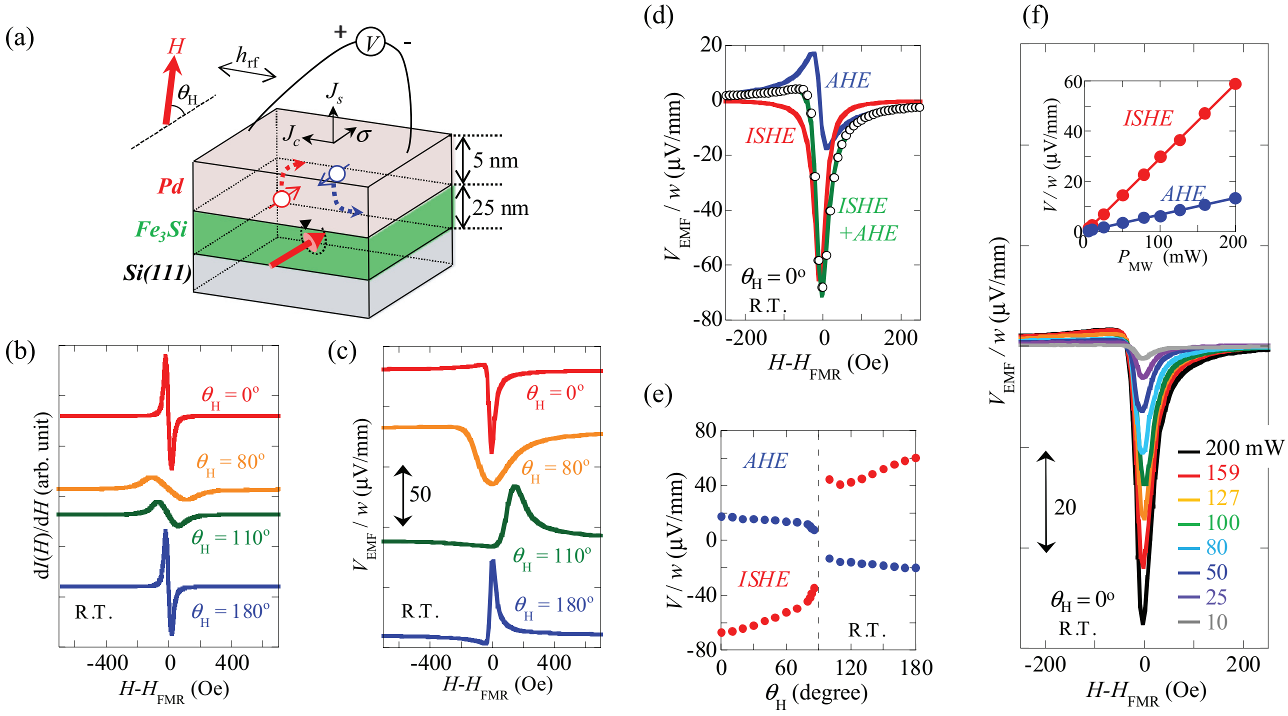

FIG. 1. (Color online) (a) Schematic illustration of the Pd/Fe$_3$Si/Si sample structure. The lateral dimensions of the Fe$_3$Si layer were 2 mm × 1 mm and the thickness d was 25 nm. The electrode separation w was 1.0 mm. The static external magnetic field H was applied at an angle of θ_H to the Fe$_3$Si film plane. (b) FMR spectra $dI(H)/dH$ for the Fe$_3$Si sample at $\theta_H = 0^\circ$, 80°, 110°, and 180° as a function of H-H_{FMR}, where I is the microwave absorption intensity in arbitrary unit. The microwave power was 200 mW. (c) Dependence of the electromotive force V_{EMF}/w on H-H_{FMR} for $\theta_H = 0^\circ$, 80°, 110°, and 180°. (d) Dependence of the electromotive force V_{EMF}/w on H-H_{FMR} for $\theta_H = 0^\circ$. The open circles are experimental data, and the green solid line is a fit obtained using Eq. (1) considering the contributions from the ISHE and AHE. The red and blue lines are fits for the ISHE signal from the Pd layer and the AHE signal from the Fe$_3$Si layer, respectively. (e) Dependence of V_{ISHE}/w and V_{AHE}/w on the magnetic field angle θ_H, where V_{ISHE} and V_{AHE} are the electromotive forces due to the ISHE and the AHE, respectively. (f) Dependence of V_{EMF}/w on H-H_{FMR} for different microwave powers at $\theta_H = 0^\circ$. The inset shows the microwave power dependence of V_{ISHE}/w and V_{AHE}/w.

where Γ is the damping constant. As shown in Fig. 1(d), a theoretical fit using Eq. (1) reproduces good agreement with the experimental results. V_{ISHE}/w and V_{AHE}/w are estimated to be 67.1 and 17.5 μV/mm, respectively. Figure 1(e) shows V_{ISHE}/w and V_{AHE}/w as a function of θ_H. The polarity reversal observed for V_{ISHE}/w when θ_H is changed from 0° to 180° is consistent with the theoretically predicted symmetry of the ISHE, expressed as $J_c = J_s \times \sigma$, where σ, J_s, and J_c are the direction of the spin, spin-current density, and charge current density,[8] respectively, thus indicating successful dynamical spin injection into the Pd layer from the Fe$_3$Si layer. This is also supported by the linear relationship between V_{ISHE}/w and the microwave power P_{MW}, shown in the inset of Fig. 1(f) [see also SM B (Ref. 19)]. Since the conductances of the Pd and Fe$_3$Si layers are in parallel to each other, the electromotive force generated in the Fe$_3$Si layer is also detected. Although the anisotropic magnetoresistance (AMR) effect can produce signals with a Lorentzian line shape in the V_{EMF}/w-H curve, the θ_H dependence of V_{ISHE}/w induced by the AMR is quite different from that shown in Fig. 1(e).[26] In addition, no such Lorentzian line shape was obtained for the Fe$_3$Si layer in the absence of the Pd layer [see SM C (Ref. 19)]. Considering these results, it can be concluded that the contribution of the AMR effect is negligibly small. Furthermore, although the temperature gradient, which can lead to an additional dc electromotive force due to the Seebeck effect, the spin Seebeck effect,[16] and the anomalous Nernst-Ettingshausen effect,[27,28] is induced in the sample in the FMR condition, these contributions were also found to be negligible [see SM C (Ref. 19)]. Therefore, it can be concluded that the origin of V_{ISHE}/w is the ISHE in the Pd layer due to a pure spin current generated by spin pumping of the Fe$_3$Si layer. In fact, when the nonmagnetic (NM) layer was changed from Pd to Al, in which spin-orbit interactions are weaker than in Pd, V_{ISHE}/w was drastically reduced to 4.20 μV/mm, which is 6.25% of the value for the Pd/Fe$_3$Si/Si sample [see SM D (Ref. 19)].

For comparison, the spin-injection efficiency was investigated for several FM materials: Ni$_{80}$Fe$_{20}$ (Py), polycrystalline Fe$_3$Si, and single-crystal Co$_6$Fe$_4$. The polycrystalline Py and Fe$_3$Si layers were fabricated on thermally oxidized Si(100) substrates (oxide thickness 500 nm). After the substrates were cleaned with acetone and isopropanol, 25-nm-thick polycrystalline Py and Fe$_3$Si layers were deposited at room temperature by EB evaporation and pulsed laser deposition (PLD), respectively. The single-crystal Co$_6$Fe$_4$ was grown by MBE.[29] After deposition of the ferromagnetic layer, a polycrystalline Pd layer was deposited using EB evaporation at room temperature. To distinguish between the single-crystal Fe$_3$Si grown by MBE and the polycrystalline Fe$_3$Si grown by PLD, these layers are referred to as "single-Fe$_3$Si"

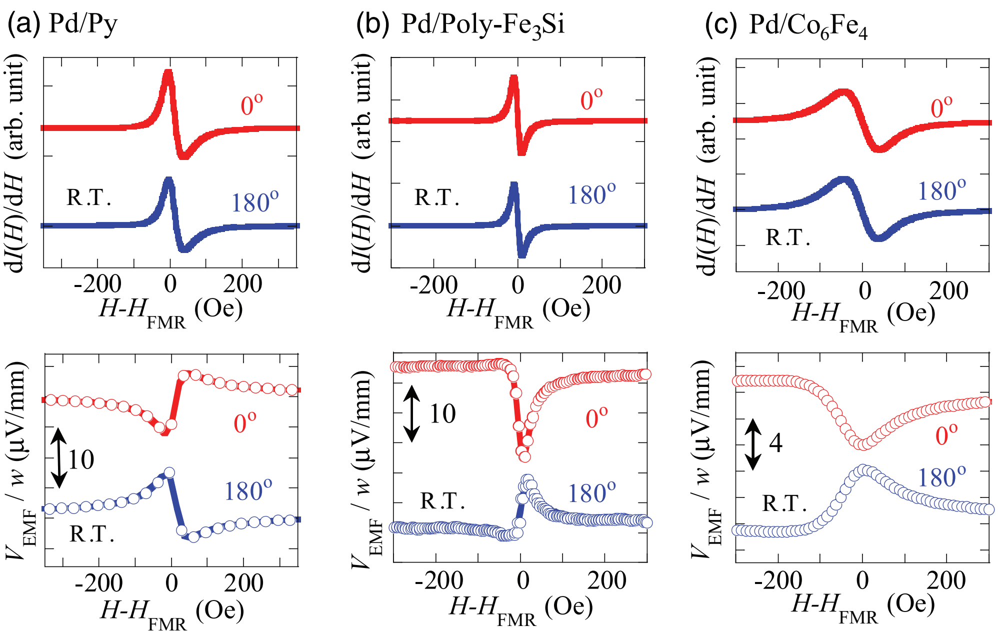

FIG. 2. (Color online) H dependence of the (top) FMR signal $dI(H)/dH$ and the (bottom) electromotive force $V_{\rm EMF}/w$ at $\theta_{\rm H} = 0^\circ$ and 180° for (a) Pd/Py/SiO$_2$/Si, (b) Pd/poly-Fe$_3$Si/SiO$_2$/Si, and (c) Pd/Co$_6$Fe$_4$/Si samples. The microwave excitation power was 200 mW. The FMR and EMF measurement procedures and the sample geometry were the same as those for the Pd/single-crystal Fe$_3$Si/Si sample shown in Fig. 1(a).

and "poly-Fe$_3$Si", respectively. Figure 2 shows the H dependence of the (top) FMR signal $dI(H)/dH$ and the (bottom) electromotive force $V_{\rm EMF}$ for $\theta_{\rm H} = 0^\circ$ and 180°, for Pd/Py/SiO$_2$/Si [Fig. 2(a)], Pd/poly-Fe$_3$Si/SiO$_2$/Si [Fig. 2(b)], and Pd/Co$_6$Fe$_4$/Si [Fig. 2(c)]. The microwave excitation power was 200 mW. Clear FMR signals and EMFs were obtained for all samples. In order to estimate the generated spin-current density J_s^0, the following equation was used:[9]

$$\frac{V_{\rm ISHE}}{w} = \frac{\theta_{\rm SHE}\lambda_N \tanh\left(\frac{d_N}{2\lambda_N}\right)}{d_N\sigma_N + d_F\sigma_F}\left(\frac{2e}{\hbar}\right) J_s^0, \qquad (2)$$

where d_F and σ_F are the thickness and electric conductivity of the FM layer and d_N, σ_N are those of the Pd layer, and λ_N and $\theta_{\rm SHE}$ is the spin diffusion length and spin Hall angle, respectively. Here, $\lambda_N = 9$ nm and $\theta_{\rm SHE} = 0.017$ were used.[9,14] From the $V_{\rm EMF}/w$ vs H curves, $V_{\rm ISHE}/w$ for the Pd/Py, Pd/poly-Fe$_3$Si, and Pd/Co$_6$Fe$_4$ samples was estimated to be 2.85, 15.0, and 2.92 μV/mm, respectively. Surprisingly, $V_{\rm ISHE}/w$ for the single-Fe$_3$Si sample (67.1 μV/mm) is more than 20 times higher than that for samples using a conventional FM material such as Py. From Eq. (2), J_s^0 for the single-Fe$_3$Si, poly-Fe$_3$Si, Py, and Co$_6$Fe$_4$ samples is calculated to be 2.75×10^{-8}, 3.91×10^{-9}, 1.25×10^{-9}, and 1.76×10^{-9} J/m^2, respectively (see Table I). Thus, for the single-Fe$_3$Si sample, the generated spin current is more than 20 times higher than that for the Py samples. Since J_s^0 is a good indicator of the spin-injection efficiency, these results clearly indicate that highly efficient spin injection is realized for the single-Fe$_3$Si sample. In general, J_s^0 is expressed as[9]

$$J_s^0 = \frac{g_r^{\uparrow\downarrow}\gamma^2 h^2 \hbar\left[4\pi M_s\gamma + \sqrt{(4\pi M_s)^2\gamma^2 + 4\omega^2}\right]}{8\pi\alpha^2\left[(4\pi M_s)^2\gamma^2 + 4\omega^2\right]}, \qquad (3)$$

where $h, \hbar, g_r^{\uparrow\downarrow}, M_\sigma$, and α are the microwave magnetic field, the Dirac constant, the real part of the mixing conductance, the saturation magnetization, and the Gilbert damping constant, respectively. ω $(=2\pi f)$ is the angular frequency of the magnetization precession, where f is the microwave frequency. The estimated $g_r^{\uparrow\downarrow}$ values and other physical parameters for the different samples are summarized in Table I. The parameters α and M_s are estimated from the width of the FMR spectrum and $H_{\rm FMR}$, respectively. These parameters are strongly dependent on the FM layer, and Eq. (3) implies that for high spin-injection efficiency, α should be as small as possible and M_s should be optimized to maximize J_s^0. However, even though the α values for the poly-Fe$_3$Si sample are smaller than those for the single-Fe$_3$Si sample, and the M_s value is comparable, J_s^0 for the poly-Fe$_3$Si sample is considerably smaller than that for the single-Fe$_3$Si sample. This indicates that α and M_s are not the main factors responsible for the large $V_{\rm ISHE}/w$ for the single-Fe$_3$Si sample. We therefore focus on $g_r^{\uparrow\downarrow}$, which is generally related to the conductance between noncollinear FMs. In this Rapid Communication, since $g_r^{\uparrow\downarrow}$ is calculated using Eq. (3), other extrinsic contributions that affect the spin-injection efficiency, which are not considered in the conventional theory, are also included in $g_r^{\uparrow\downarrow}$. As can be seen from Table I, $g_r^{\uparrow\downarrow}$ for the single-Fe$_3$Si sample is clearly larger than those for the other samples. It should also be noted that $g_r^{\uparrow\downarrow}$ for the Co$_6$Fe$_4$ sample is also relatively large despite the small J_s^0 value. Both of these results were reproducible over several samples. This unexpected behavior of $g_r^{\uparrow\downarrow}$ might provide an important clue to understanding the mechanism that gives rise to the large $V_{\rm ISHE}$ for the single-Fe$_3$Si sample.

Based on the results shown in Table I, a possible mechanism is now considered. Figure 3 schematically illustrates the

TABLE I. Physical parameters for estimating J_s^0 and $g_r^{\uparrow\downarrow}$ of different ferromagnetic samples. M_s and α were obtained from H_{FMR} and the linewidth of the FMR spectrum, respectively. The conductivity and spin diffusion length for the Pd layer are $4.08 \times 10^6\ \Omega^{-1}\ \mathrm{m}^{-1}$ and 9 nm, respectively, as reported in Refs. 9 and 14.

		M_s (emu/cc)	α	σ_{F} (Ω^{-1} m^{-1})	J_s^0 (J/m^2)	$g_r^{\uparrow\downarrow}$ (m^{-2})
Fe$_3$Si	Single crystalline	828	0.0087	1.25×10^6	2.75×10^{-8}	6.2×10^{20}
Fe$_3$Si	Polycrystalline	860	0.0050	0.910×10^6	3.91×10^{-9}	2.3×10^{19}
Py	Polycrystalline	535	0.0149	2.50×10^6	1.25×10^{-9}	5.2×10^{19}
Co$_6$Fe$_4$	Single crystalline	1600	0.0227	5.00×10^6	1.76×10^{-9}	3.1×10^{20}

spin-current flow generated by spin pumping in samples consisting of NM and FM layers, for different interface conditions between the FM layer and the substrate. Figure 3(a) shows the case for a single FM layer with an atomically flat interface with the substrate, Fig. 3(b) shows the case for a rough interface between a single FM layer and the substrate, and Fig. 3(c) shows a situation where there are two different FM layers with different saturation magnetizations, and an atomically flat interface exists between the lower FM2 layer and the substrate. Although the ideal spin pumping condition is represented by Fig. 3(a), it is possible that a nonzero interface roughness exists between FM1 layer and the substrate as shown in Fig. 3(b). In this case, since the ferromagnetic resonance condition of the magnetization near the interface is changed due to shape anisotropy,[14] the magnetization near the interface does not precess under the same FMR condition as that for the FM1 layer. Since the spin diffusion length in FM1 layer is short, the FM1 layer near the interface in Fig. 3(b) can act as an effective spin sink, resulting in a reduction of the spin current flowing into the NM layer. Such a region also induces an additional EMF, which can cause a significant change in the measured V_{ISHE}/w. A similar situation should occur for the sample shown in Fig. 3(c), with an atomically flat FM2 layer. Here, Fig. 3(a) corresponds to the case for the single-Fe$_3$Si and the Co$_6$Fe$_4$ samples, and Fig. 3(b) corresponds to the case for the Py and poly-Fe$_3$Si samples because the thermally oxidized Si substrate has a nonzero surface roughness. In fact, a measurable V_{ISHE}/w was found for a Py layer without any NM layer, which indicates the existence of another spin sink.[30] Although the Co$_6$Fe$_4$ sample also has an ideal atomically flat interface, across which spins can be electrically injected from the Co$_6$Fe$_4$ into a Si channel even at room temperature,[31,32] the large α and M_s values lead to a significant reduction in the spin-current density, as indicated by Eq. (3). Thus, $g_r^{\uparrow\downarrow}$ might also reflect the crystal and magnetic quality of the ferromagnetic layer.[33,34]

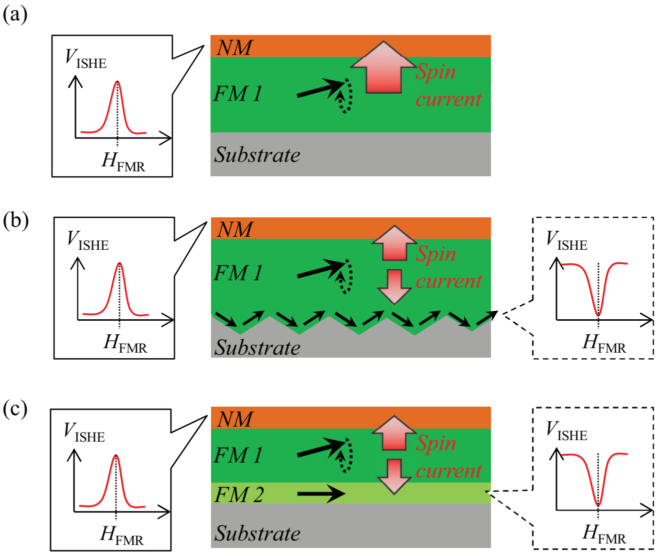

FIG. 3. (Color online) Schematic illustration of spin-current flow under FMR conditions for samples with different interface structures between the FM layer and substrate: (a) An atomically flat interface, (b) a rough interface, and (c) an atomically flat interface with an interfacial FM2 layer whose saturation magnetization is different from that of the FM1 layer. The schematics show the spin-current flow under FMR conditions for the FM1 layer. The upper figure represents ideal spin pumping conditions.

To experimentally investigate whether this was in fact the case, two control experiments are carried out using single-Fe$_3$Si samples with different interfacial conditions. First, an as-grown single-Fe$_3$Si/Si sample was annealed at 350 °C for 30 min. in an Ar atmosphere because an earlier study revealed that slight intermixing occurs between the Fe$_3$Si layer and the Si substrate at around 300 °C.[25] Cross-sectional transmission electron microscopy images of the as-grown and annealed Fe$_3$Si/Si samples are shown in Figs. 4(a) and 4(b), respectively. An atomically flat interface is formed in the as-grown sample, whereas the interfacial layer whose thickness is spatially varied from 1 to 5 nm is formed after annealing. Thus, the annealed sample is expected to have a rough interfacial layer, which corresponds both to the sample in Fig. 3(b) and that in Fig. 3(c). Following annealing, a 5-nm-thick Pd layer was deposited. FMR spectra for the as-grown and annealed samples are shown in Fig. 4(c). To highlight the differences in the FMR field between these two samples, the microwave absorption intensity I, rather than dI/dH, is plotted as a function of H-H_{FMR}. As indicated by the blue arrow, the absorption intensity under a high external magnetic field which corresponds to small magnetization is enhanced for the annealed sample, indicating the presence of a Si-rich interfacial layer. Figure 4(d) shows V_{EMF}/w against H-H_{FMR} for the annealed sample, measured at $\theta_{\mathrm{H}} = 0^\circ$ and 180°. The microwave excitation power was 200 mW. The signal shape is seen to be significantly different from that for the as-grown sample shown in Fig. 1(c). The magnitude of V_{ISHE}/w was estimated to be 12.6 μV/mm, which is about 20% of that for

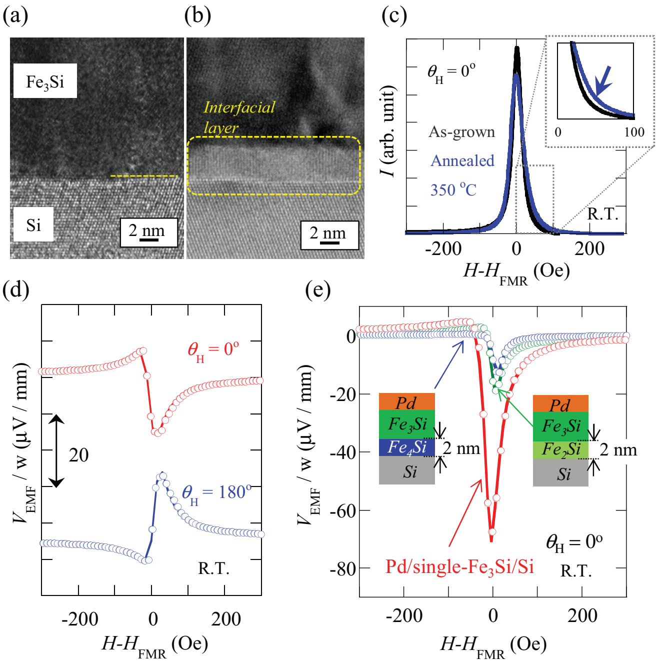

FIG. 4. (Color online) Cross-sectional transmission electron microscopy images of (a) as-grown and (b) annealed Fe_3Si/Si samples. (c) FMR spectra for an as-grown Pd/Fe_3Si/Si sample and sample annealed at 350 °C for 30 min. in an Ar atmosphere. The expanded graph is shown in the inset. (d) V_{EMF}/w for the annealed sample at $\theta_H = 0^\circ$ and 180°. The microwave excitation power was 200 mW. The EMF measurement procedure and the sample geometry were the same as those for the Pd/single-Fe_3Si/Si sample. The open circles are experimental data and the solid line is a fit obtained using Eq. (1). (e) V_{EMF}/w for Pd/Fe_3Si(23 nm)/$Fe_{3-x}Si_{1+x}$(2 nm)/Si samples at $\theta_H = 0^\circ$. The microwave excitation power was 200 mW. The composition of the 2-nm-thick interfacial layer is either Fe_4Si (blue) or Fe_2Si (green). A representative V_{EMF}-H curve for the Pd/Fe_3Si(25 nm)/Si sample is displayed using red circles. The open circles are experimental data and the solid line is a fit obtained using Eq. (1).

the as-grown sample. A second control experiment is carried out by using an intentionally inserted additional FM layer near the interface with the substrate, as in Fig. 3(c). In these samples, a 2-nm-thick layer of either Fe_4Si or Fe_2Si was grown on the substrate before growth of the single-Fe_3Si layer. Despite the large composition change, no evidence was found that the presence of such an interfacial layer affected the epitaxial growth of the single-Fe_3Si layer, and the interfaces remained atomically flat. Figure 4(e) shows V_{EMF}/w against H-H_{FMR} for these two samples. The magnitude of V_{ISHE} was drastically reduced to 13.2 μV/mm for the sample with Fe_4Si and 16.2 μV/mm for the sample with Fe_2Si, despite the presence of atomically flat interfaces. The results shown in Fig. 4 strongly support the idea that to realize highly efficient spin injection using spin pumping techniques, magnetic properties of the FM layer near the interface should be carefully considered. These findings are likely to have a major impact in the field of spintronics. We believe that further enhancement of the spin-injection efficiency can be realized by using completely uniform FM metals with a much smaller α value, such as Co-based Heusler alloys.

In summary, we have demonstrated spin pumping using a single-crystalline Fe_3Si layer. The generated spin current in the Pd/Fe_3Si/Si sample was estimated to be 20-fold, compared with that of conventional ferromagnetic materials such as Py. A high-quality single crystal of Fe_3Si with uniform ferromagnetic properties allowed us to suppress spin current absorbed by an unexpected spin reservoir, such as an interfacial ferromagnetic layer with different ferromagnetic properties, resulting in a marked enhancement of spin-injection efficiency.

This research was supported in part by a Grant-in-Aid for Scientific Research from the MEXT, Japan, by STARC, by the Adaptable & Seamless Technology Transfer Program through Target-driven R&D from JST, and by the Toray Science Foundation.

---

[*] Corresponding author: ando@ee.es.osaka-u.ac.jp

[1] S. A. Wolf, D. D. Awschalom, R. A. Buhrman, J. M. Daughton, S. von Molnar, M. L. Roukes, A. Y. Chtchelkanova, and D. M. Treger, Science **294**, 1488 (2001).

[2] M. Johnson and R. H. Silsbee, Phys. Rev. Lett. **55**, 1790 (1985).

[3] F. J. Jedema, A. T. Filip, and B. J. van Wees, Nature (London) **410**, 345 (2001).

[4] T. Kimura, N. Hashimoto, S. Yamada, M. Miyao, and K. Hamaya, NPG Asia Mater. **4**, e9 (2012).

[5] S. Mizukami, Y. Ando, and T. Miyazaki, Phys. Rev. B **66**, 104413 (2002).

[6] Y. Tserkovnyak, A. Brataas, and G. E. W. Bauer, Phys. Rev. Lett. **88**, 117601 (2002).

[7] A. Brataas, Y. Tserkovnyak, G. E. W. Bauer, and B. I. Halperin, Phys. Rev. B **66**, 060404(R) (2002).

[8] E. Saitoh, M. Ueda, H. Miyajima, and G. Tatara, Appl. Phys. Lett. **88**, 182509 (2006).

[9] K. Ando and E. Saitoh, J. Appl. Phys. **108**, 113925 (2010).

[10] K. Ando, S. Takahashi, J. Ieda, H. Kurebayashi, T. Trypiniotis, C. H. W. Barnes, S. Meakawa, and E. Saitoh, Nat. Mater. **10**, 655 (2011).

[11] E. Shikoh, K. Ando, K. Kubo, E. Saitoh, T. Shinjo, and M. Shiraishi, Phys. Rev. Lett. **110**, 127201 (2013).

[12] M. Koike, E. Shikoh, Y. Ando, T. Shinjo, S. Yamada, K. Hamaya, and M. Shiraishi, Appl. Phys. Express **6**, 023001 (2013).

[13] Z. Y. Tang, E. Shikoh, H. Ago, K. Kawahara, Y. Ando, T. Shinjo, and M. Shiraishi, Phys. Rev. B **87**, 140401(R) (2013).

[14] Y. Kitamura, E. Shikoh, Y. Ando, T. Shinjo, and M. Shiraishi, Sci. Rep. **3**, 1739 (2013).

[15] Z. Y. Tang, Y. Kitamura, E. Shikoh, Y. Ando, T. Shinjo, and M. Shiraishi, Appl. Phys. Express **6**, 083001 (2013).

[16] K. Uchida, S. Takahashi, K. Harii, J. Ieda, W. Koshibae, K. Ando, S. Maekawa, and E. Saitoh, Nature (London) **455**, 778 (2008).

[17] K. Uchida, H. Adachi, T. An, T. Ota, M. Toda, B. Hillebrands, S. Maekawa, and E. Saitoh, Nat. Mater. **10**, 737 (2011).

[18] T. Kimura, J. Hamrle, and Y. Otani, Phys. Rev. B **72**, 014461 (2005).

[19] See Supplemental Material at http://link.aps.org/supplemental/10.1103/PhysRevB.88.140406 for control experiments.

[20] K. Hamaya, K. Ueda, Y. Kishi, Y. Ando, T. Sadoh, and M. Miyao, Appl. Phys. Lett. **93**, 132117 (2008).

[21] T. Sadoh, M. Kumano, R. Kizuka, K. Ueda, A. Kenjo, and M. Miyao, Appl. Phys. Lett. **89**, 182511 (2006).

[22] J. Herfort, H. P. Schonherr, and K. H. Ploog, Appl. Phys. Lett. **83**, 3912 (2003).

[23] Y. Ando, K. Hamaya, K. Kasahara, Y. Kishi, K. Ueda, K. Sawano, T. Sadoh, and M. Miyao, Appl. Phys. Lett. **94**, 182105 (2009).

[24] Y. Ando, K. Kasahara, K. Yamane, K. Hamaya, K. Sawano, T. Kimura, and M. Miyao, Appl. Phys. Express **3**, 093001 (2010).

[25] Y. Ando, K. Hamaya, K. Kasahara, K. Ueda, Y. Nozaki, T. Sadoh, Y. Maeda, K. Matsuyama, and M. Miyao, J. Appl. Phys. **105**, 07B102 (2009).

[26] W. G. Egan and H. J. Juretschke, J. Appl. Phys. **34**, 1477 (1963).

[27] S. Y. Huang, W. G. Wang, S. F. Lee, J. Kwo, and C. L. Chien, Phys. Rev. Lett. **107**, 216604 (2011).

[28] M. Weiler, M. Althammer, F. D. Czeschka, H. Huebl, M. S. Wagner, M. Opel, I.-M. Imort, G. Reiss, A. Thomas, R. Gross, and S. T. B. Goennenwein, Phys. Rev. Lett. **108**, 106602 (2012).

[29] Y. Maeda, K. Hamaya, S. Yamada, Y. Ando, K. Yamane, and M. Miyao, Appl. Phys. Lett. **97**, 192501 (2010).

[30] A. Tsukahara, Y. Kitamura, E. Shikoh, Y. Ando, T. Shinjo, and M. Shiraishi, arXiv:1301.3580.

[31] Y. Ando, Y. Maeda, K. Kasahara, S. Yamada, K. Masaki, Y. Hoshi, K. Sawano, K. Izunome, A. Sakai, M. Miyao, and K. Hamaya, Appl. Phys. Lett. **99**, 132511 (2011).

[32] Y. Ando, K. Kasahara, S. Yamada, Y. Maeda, K. Masaki, Y. Hoshi, K. Sawano, M. Miyao, and K. Hamaya, Phys. Rev. B **85**, 035320 (2012).

[33] X. Jia, K. Liu, K. Xia, and G. E. W. Bauer, Europhys. Lett. **96**, 17005 (2011).

[34] Z. Qiu, K. Ando, K. Uchida, Y. Kajiwara, R. Takahashi, H. Nakayama, T. An, Y. Fujikawa, and E. Saitoh, Appl. Phys. Lett. **103**, 092404 (2013).